Simulation of Paddling on Ergometer

M. BEGON* and Ph. SARDAIN**

** School of Sport and Exercise Sciences, Loughborough University Loughborough Leics LE11 3TU (United Kingdom) M.Begon@lboro.ac.uk*
*** Laboratoire de Mécanique des Solides, UMR 6610, CNRS, Université de Poitiers*
SP2MI, Bd Marie et Pierre Curie, Téléport 2, BP 30179 86962 Futuroscope Chasseneuil Cedex (France) sardain@lms.univ-poitiers.fr

Abstract. The simulation of sports movements on ergometer can predict the effects of both material and technical changes. Our aim is to present a simulation model of paddling on an ergometer with sliding footrest-seat complex. The system "ergometer-athlete-paddle" has 31 degrees of freedom and 2 kinematic closed-loops. The input parameters are the geometrical and anthropometrical models and the trunk and paddle kinematics. The dynamic model of the ergometer is defined by functions of the generalized coordinates and their first and second time derivatives. The kayaker's kinematics are obtained by solving an inverse kinematics problem. The anteroposterior acceleration of the sliding complex depends on the state variables, the contact forces applied to the paddle tips and the tension of the bungee linking the ergometer to the sliding complex. The forward dynamics analysis solves for the state variables of the sliding complex. Subsequently the contact forces and the joint torques are estimated by solving an inverse dynamics problem.

1. Introduction

Mathematical modelling and computer simulation play an increasingly important role in the search for answers to questions that cannot be addressed experimentally. The main purposes are the analysis of musculo-skeletal co-ordinations (*e.g.* van Soest *et al.*, 2005), the explanation of sports techniques (*e.g.* Yeadon and Hiley, 2000) or the optimization of the performance (*e.g.* Yeadon and Brewin, 2003). Often the movement is considered as 2D motion and the number of degrees of freedom is restricted.

The ergometers are also used when the *in situ* experimental conditions are a problem. In aquatic activities like kayaking or rowing, the main difficulty is the 3D kinematics acquisition. Before any interpretation may be made, the ergometer has to respect the kinematics and the dynamics of the actual movement. An experimental validation is necessary. However an analysis of the differences is not enough for ergometer improvement. The simulation becomes a helpful tool also for optimizing ergometer design.

The kinematic tasks of the activity can be acquired *in situ*. Then the results of the ergometer simulation driven by these kinematic tasks can be compared with actual results (*e.g.* acceleration of the system athlete-boat or the external forces). The purpose of this study is to present the simulation of paddling on a kayak ergometer with a sliding footrest and seat complex. The aim of the sliding complex is to reproduce the kayak acceleration in order to respect the kayaking dynamics.

Section 2 presents briefly the ergometer and section 3 describes the geometrical model. Sections 4, 5 and 6 focus on the three steps of the simulation: the inverse kinematics problem to obtain the kayaker kinematics from kayaking tasks, the forward dynamics problem to simulate the sliding complex kinematics and the inverse dynamics problem to calculate the joint torques.

2. Ergometer with a sliding footrest and seat complex

A kayak ergometer was designed using a static frame on which a trolley (*i.e.* footrest and seat complex) moved back and forth (Fig. 1). A bungee cord linked the back of the frame with the trolley. An air brake simulated the water drag on the blade. The paddle was linked to the air brake by two ropes. Because of 1the freewheel pulley, the rope drove the flywheel if its angular velocity was higher than the shaft velocity. When the rope unwound, an elastic cord wound round the pulley. During the return of the blade, the tension of the elastic cord wound the rope. Between two strokes, the flywheel resistance decelerated the shaft.

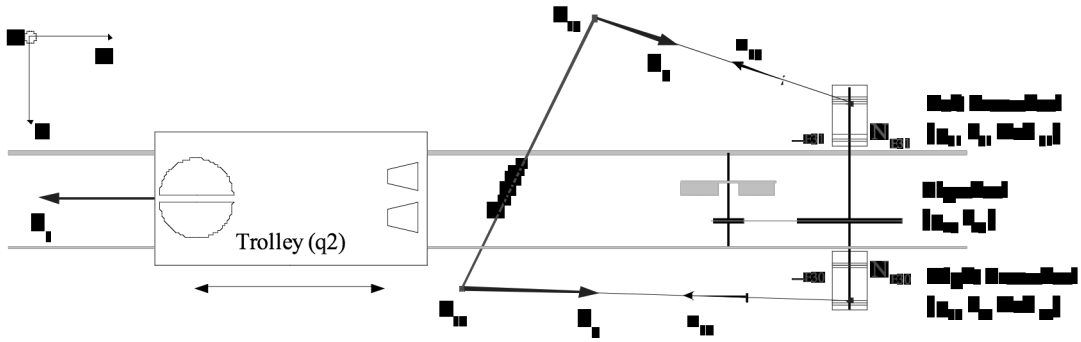

Figure 1. Schematic diagram and notations of the ergometer with sliding trolley and the air brake (upper view).

3. Ergometer-kayaker model

The model "ergometer-kayak" was implemented under *HuMAnS* (Wieber et al., 2006). The dynamics was represented as Lagrangian dynamics with Lagrange multipliers for introducing the contacts forces:

$$\mathbf{M}(\mathbf{q})\ddot{\mathbf{q}} + \mathbf{N}(\mathbf{q},\dot{\mathbf{q}})\dot{\mathbf{q}} + \mathbf{G}(\mathbf{q}) = \hat{\mathbf{o}} + \mathbf{C}^T\ddot{\mathbf{e}} \quad (1)$$

where the vector $\mathbf{q}, \dot{\mathbf{q}}$ and $\ddot{\mathbf{q}}$ represent the generalized coordinates, their speed and acceleration. $\mathbf{M}(\mathbf{q}), \mathbf{N}(\mathbf{q},\dot{\mathbf{q}})$ and $\mathbf{G}(\mathbf{q})$ are the inertia matrix, the other inertial nonlinear effects (Coriolis and centrifugal forces) and the gravity effects respectively. The vector $\boldsymbol{\tau}$ represents the joint torques and $\mathbf{C}^T\ddot{\mathbf{e}}$ the contact forces. The analytical models of the dynamics were based on state-of-art algorithms described in Featherstone and Orin (2000).

The kayaker-paddle-trolley model was composed of 18 bodies (Fig. 2). 22 degrees of freedom (DoF) described the kayaker movement ($\mathbf{q1}=[q_1 \ldots q_{22}]^T$). Due to the numerous contacts with the trolley and the paddle, there were 2 closed-loops (i.e. the upper and lower limbs). Two half-paddles were modelled. They were linked by a revolute joint that it used to close the kinematic loop of the upper limbs.

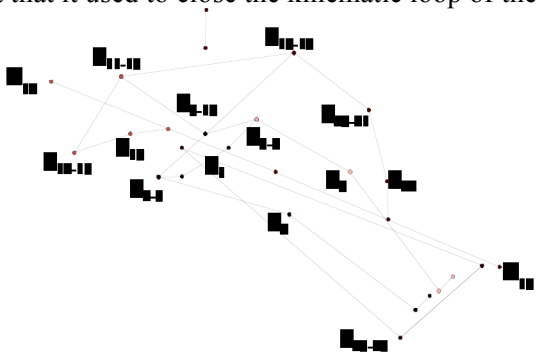

Figure 2. Schematic diagram of the system "athlete-trolley":
q_i represents the degrees of freedom et T_i the tags for describing the segments.

6 additional DoF represented the position and orientation of the trolley ($\mathbf{q2}=[q_{23} \ldots q_{28}]^T = [0\ 0\ 0\ q26\ 0\ 0]^T$). On the present ergometer, only the anteroposterior translation of the root could vary. The state of the air brake (the flywheel and the two pulleys) was given by 3 extra DoF.

4. Inverse kinematics problem: calculation of q1

4.1 *Kinematic tasks*

The kinematic tasks have to characterize the performance and the technique of the kayakers. The performance is associated with the paddle trajectory. This trajectory was defined by the time histories of the spatial position of the paddle middle and the spherical coordinates (azimuth and elevation) of the paddle. According to a kinematics analysis of 12 elite kayakers, the main difference was the rotation of the pelvic and scapular girdles. Both parameters (q_1 and q_{10}) were chosen. The tasks (x) for each kayaker were fitted by Fourier series:

$$x = c_1 + c_2\cos(\beta) + c_3\sin(\beta) + c_4\cos(2\beta) + c_5\sin(2\beta) \quad (2)$$

4.2 *Lower limbs solving*

The lower limbs closed-loop has as many DoF (7) as the task defined by the pelvis rotation and the 3D position of the feet. The generalized coordinates were solved by an iterative procedure, based on the Newton-Raphson approach. By inversion of the Jacobian matrix ($J_{i,j}= \partial x_i/q_j$), q were adjusted until satisfying the task equation. The Jacobian matrix was computed by analytical differentiation.

4.3 *Upper limbs solving*

For the upper limbs the control space is larger than the task space. The problem was solved by introducing a damped pseudo-inverse of J ($J^{+\lambda}$) and an optimization term. The damped pseudo-inverse was calculated from a trimmed-down version of the singular value decomposition. The null space of the Jacobian matrix was used to optimize a secondary task by projection of its gradient. The chosen function (Fournier, 1980) kept the joint angles as far as possible to the joint limits. The adjustment of q was expressed by:

$$\Delta q = J^{+\lambda}\Delta x + (1 - J^{+}J)\frac{2\alpha(q_i - \overline{q}_i)}{\Delta q_i^2} \quad (3)$$

where α is the weighting between the first and the second tasks; Δq_i is the range of motion of the joint i and $\overline{q}_i$ its average position.

5. Forward dynamic problem: calculation of q2

5.1 *Dynamic model of the kayaker*

The aim of the simulation was to calculate the state of the trolley $(\mathbf{q2}, \dot{\mathbf{q}}\mathbf{2})$ according to the kayaker movement. The trolley acceleration had to be determined from the dynamics and then integrated.

The inertia parameters (mass, position of the centre of mass and moment of inertia) of the segments were calculated using the table of de Leva (1996). The segment length and the mass of the body were measured for each kayaker.

5.2 *Dynamic model of the ergometer*

The contact forces of the system "athlete-paddle-trolley" are forces applied on the paddle tips (λ_2 and λ_3) and the tension of the bungee cord linking the trolley to the frame (λ_1). This last force was expressed as a function of the trolley position:

$$\lambda_1 = a_3 q_{26}^3 + a_2 q_{26}^2 + a_1 q_{26} \equiv O_1 \quad (4)$$

According to the mechanism of the air brake described in section 2 (Fig. 1), the paddle tip force comes from the tension of elastic cord, the air brake resistance, the pulley radius and the time derivative of the air brake angular momentum. The time derivatives of the angular momentum of the air brake (δ_{29}, δ_{30} and δ_{31}) were written according 3 different cases:

- The shaft is driven by the right pulley:

$$\begin{cases} \delta_{29+30} = (I_{29} + I_{30})\ddot{q}_{30} = \tau_{E_{30}} + \tau_{29} + \dfrac{u^x_{14}}{\mathrm{Rad}_{30}}\lambda_2 \\ \delta_{31} = I_{31}\ddot{q}_{31} = \tau_{E_{31}} + \dfrac{u^x_{19}}{\mathrm{Rad}_{31}}\lambda_3 \end{cases} \quad (5)$$

- The shaft is driven by the left pulley:

$$\begin{cases} \delta_{29+31} = (I_{29} + I_{31})\ddot{q}_{31} = \tau_{E_{31}} + \tau_{29} + \dfrac{u^x_{19}}{\mathrm{Rad}_{31}}\lambda_3 \\ \delta_{30} = I_{30}\ddot{q}_{30} = \tau_{E_{30}} + \dfrac{u^x_{14}}{\mathrm{Rad}_{30}}\lambda_2 \end{cases} \tag{6}$$

- The shaft is not driven:

$$\begin{cases} \delta_{29} = I_{29}\ddot{q}_{29} = \tau_{29} \\ \delta_{30} = I_{30}\ddot{q}_{30} = \tau_{E_{30}} + \dfrac{u^x_{14}}{\mathrm{Rad}_{30}}\lambda_2 \\ \delta_{31} = I_{31}\ddot{q}_{31} = \tau_{E_{31}} + \dfrac{u^x_{19}}{\mathrm{Rad}_{31}}\lambda_3 \end{cases} \tag{7}$$

where I is the inertia of each part (Fig. 1), τ_{29}, τ_{E30} and τ_{E31} are the air brake resistance torque and the torque due to the elastic tension for the right and left pulleys of radius Rad_{30} and Rad_{31} respectively. u^x_{14} and u^x_{19} represent the anteroposterior component of the unit vector of the right and left ropes.

Series of measurements with a torque transducer and an angular velocity sensor were carried out in order to determine the models. Firstly, the moment generated by the elastic cord (τ_E) depends on the number of turns around the pulley (N_E):

$$\tau_E(N_E) = a_1 \exp^{-\left(\frac{N_E - b_1}{c1}\right)^2} + a_2 \exp^{-\left(\frac{N_E - b_2}{c_2}\right)^2} \tag{8}$$

N_E is calculated from the pulley rotation (q_{30} or q_{31}). The physics of the air brake resistance is defined by:

$$\tau_{29} = p_2\dot{q}^2_{29} + p_1\dot{q}_{29} + p_0 \tag{9}$$

The second step is to expressed the pulley acceleration with respect to the known parameters (i.e. $\mathbf{q}, \dot{\mathbf{q}}, \ddot{\mathbf{q}}\mathbf{1}$) and to the unknown parameter ($\ddot{\mathbf{q}}\mathbf{2}$). Only the right side is emphasized here. The pulley velocity and acceleration depend on the paddle tip ($\mathbf{T}_{14}$) kinematics and on the rope orientation ($\mathbf{u}_{14}$):

$$\begin{aligned} \dot{q}_{30} &= \mathbf{u}^T_{14}\dot{\mathbf{T}}_{14} / \mathrm{Rad}_{30} \\ \ddot{q}_{30} &= \left(\dot{\mathbf{u}}^T_{14}\dot{\mathbf{T}}_{14} + \mathbf{u}^T_{14}\ddot{\mathbf{T}}_{14}\right) / \mathrm{Rad}_{30} \end{aligned} \tag{10}$$

By introducing a Jacobian matrix ($\mathbf{J}_{14}=[\mathbf{J}_{14,1}\ \mathbf{J}_{14,2}]= [\partial\mathbf{T}_{14}/\partial\mathbf{q}\mathbf{1}\ \partial\mathbf{T}_{14}/\partial\mathbf{q}\mathbf{2}]$) and the Hessian vector (h_{14}) which are computed by analytical differentiation, the time derivatives of T_{14} yield:

$$\begin{aligned} \dot{T}_{14} &= \mathbf{J}_{14}\dot{\mathbf{q}} \\ \ddot{T}_{14} &= \mathbf{J}_{14,1}\ddot{\mathbf{q}}\mathbf{1} + h_{14} + \mathbf{J}_{14,2}\ddot{\mathbf{q}}\mathbf{2} \end{aligned} \tag{11}$$

Eq. [10] is introduced into Eq. [9] and then $\ddot{\mathbf{q}}\mathbf{2}$ is factorized and the expression simplified:

$$\ddot{q}_{30} = A_{14} + B_{14}\ddot{\mathbf{q}}\mathbf{2} \tag{12}$$

Booleans (b_{30} and b_{31}) are introduced into Eq. [5,6,7]. Hence the expression of the force applied to the right paddle tip yields:

$$\lambda_2 = \frac{u^x_{14}}{\mathrm{Rad}_{30}}\left(\left(I_{30} + b_{30}I_{29}\right)\ddot{q}_{30} - \tau_{E_{30}} - b_{30}\tau_{29}\right) \tag{13}$$

Substituting for $\ddot{q}_{30}$ from Eq. [12] in Eq. [13], the expression of λ_2 simplifies to:

$$\lambda_2 = O_2 + P_2\ddot{\mathbf{q}}\mathbf{2} \tag{14}$$

5.3 *Trolley acceleration solving*

If we consider then the structure of the vector $\mathbf{q}$: $\mathbf{q}=[\mathbf{q}\mathbf{1}\ \mathbf{q}\mathbf{2}]^T$, we can split the dynamics (Eq. [1]) to exhibit the same structure:

$$\begin{bmatrix} \mathbf{M}_{1,1} & \mathbf{M}_{1,2} \\ \mathbf{M}_{2,1} & \mathbf{M}_{2,2} \end{bmatrix} \begin{pmatrix} \ddot{\mathbf{q}}\mathbf{1} \\ \ddot{\mathbf{q}}\mathbf{2} \end{pmatrix} + \begin{bmatrix} \mathbf{N}_1 \\ \mathbf{N}_2 \end{bmatrix} \begin{pmatrix} \dot{\mathbf{q}}\mathbf{1} \\ \dot{\mathbf{q}}\mathbf{2} \end{pmatrix} + \begin{bmatrix} \mathbf{G}_1 \\ \mathbf{G}_2 \end{bmatrix} = \begin{bmatrix} \hat{\mathbf{o}} \\ \mathbf{0} \end{bmatrix} + \begin{bmatrix} \mathbf{C}_1^T \\ \mathbf{C}_2^T \end{bmatrix} \ddot{\mathbf{e}} \tag{15}$$

where the joint torques do not appear in the lower part:

$$\begin{bmatrix} \mathbf{M}_{2,1} & \mathbf{M}_{2,2} \end{bmatrix} \begin{pmatrix} \ddot{\mathbf{q}}\mathbf{1} \\ \ddot{\mathbf{q}}\mathbf{2} \end{pmatrix} + \mathbf{N}_2\dot{\mathbf{q}} + \mathbf{G}_2 = \mathbf{C}_2^T\ddot{\mathbf{e}} \tag{16}$$

By substituting the contact force by Eq. [4] and Eq. [14], the anteroposterior acceleration of the trolley yields:

$$\ddot{q}_{26} = \frac{O_1 + O_2 + O_3 - \mathbf{N}_2\dot{\mathbf{q}} - \mathbf{G}_2 - \mathbf{M}_{2,1}\ddot{\mathbf{q}}\mathbf{1}}{\mathbf{M}_{2,2} - P_2 - P_3} \tag{17}$$

This ordinary differential equation was solved with root finding (i.e. the 3 different air brake dynamics) under *Scilab*.

6. Inverse dynamics problem

The kinematics of the whole system has been determined. Due to the two closed-loops and the three contacts between the kayaker and the trolley (two feet and the pelvis), some assumptions have to be presented for the joint torque calculation. From the lower part of the dynamics of the system "athlete-paddle" (equation analogous to Eq. [15]), the contact forces yield:

$$\begin{bmatrix} \ddot{\mathbf{e}}_a \\ \ddot{\mathbf{e}}_b \end{bmatrix} = \begin{bmatrix} \mathbf{C}_{2a} \\ \mathbf{C}_{2b} \end{bmatrix}^{-T} \left(\mathbf{M}_2\ddot{\mathbf{q}} + \mathbf{N}_2\dot{\mathbf{q}} + \mathbf{G}_2 \right) \tag{18}$$

where λ_a and λ_b represent the contact force applied to the paddle tips and to the settings, respectively. λ_a is calculated from Eq. [14] and λ_b can be estimated by introducing a weighted pseudo-inverse:

$$\ddot{\mathbf{e}}_b = \left(\mathbf{C}_{2b}^T \mathbf{W}^{-1} \mathbf{C}_{2b} \right)^{-1} \mathbf{C}_{2b}^T \mathbf{W}^{-1} \left(\mathbf{M}_2\ddot{\mathbf{q}} + \mathbf{N}_2\dot{\mathbf{q}} + \mathbf{G}_2 - \mathbf{C}_{2a}^T \ddot{\mathbf{e}}_a \right) \tag{19}$$

The weighting factors in W give penalties to anteroposterior and mediolateral components of the force applied to the seat in order to respect the unilateral contact.

7. Results – Discussion

7.1 *Kayaker kinematics*

The present simulation can be a useful tool to test material and technical changes. The kayaker kinematics is calculated from tasks that are easily acquired on ergometer or in kayak with goniometer and inertial sensors. Fig. 3 illustrates the kinematics of some joints over one cycle. The generated movement from kinematics tasks is cyclic; the final position is similar to the initial one. The joint limits are respected except for the elbow and shoulder of some kayakers. The exceeded angles come from the assumptions of a built-in joint between the hand and the paddle. The athlete does not firmly hold the paddle to increase the range of motion. The flexion-extension and lateral bending of the thorax allow all tasks to be reached. Due to approximation of paddle trajectory by Fourier series, some positions would be unreachable despite the full elbow extension and cause singularity of the Jacobian matrix. The damping pseudo-inverse which is introduced in Eq. [3] avoids this algorithm instability.

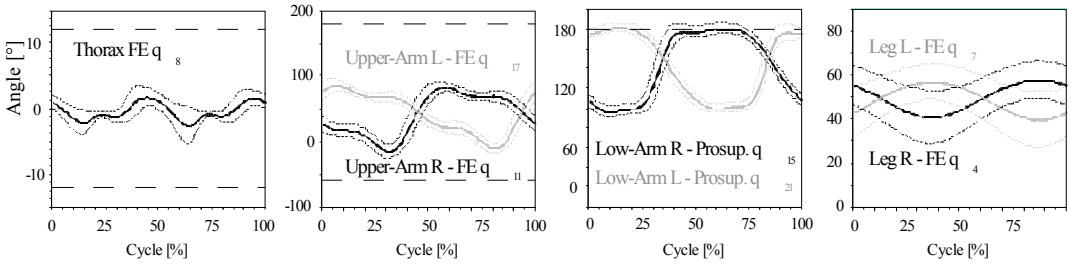

Figure 3. Times histories of the joint angles over one cycle (right and left strokes). The horizontal dashed lines or the frame represent the joint limits.

7.2 *Trolley kinematics and paddle tips force*

The range of trolley oscillations is similar to experimental data. The average forces (n=26 trials) applied to paddle tips are comparable to actual forces. However on each curve, there is a peak of force just when a pulley drives the shaft. The peak of force comes from the rigidity of the system and the kinematics fitting. The rope could be modelled as a damped linear spring (Hiley and Yeadon, 2003) and the task kinematics could be fitted by phases (catch, drive, exit and recovery) to improve the fidelity of the paddle tips acceleration.

7.3 *Contact forces and joint torques*

Despite closing the kinematic loop of the upper-limbs, no contact forces were added between the two half-paddles. With the present ergometer, these forces cannot be measured. Due to the distance between the middle of the paddle and the hand, a weak contact force has a large effect on the joint torque. The instrumentation has to be improved with a 3D force sensor between the hands. For the setting forces, the pseudo-inverse does not allow the experimental forces to be reproduced. Before any interpretation on the joint torque, some behaviour models of contact force distribution which are based on experimental data are necessary.

References

de Leva, P. (1996). Adjustments to Zatsiorsky-Seluyanov's segment inertia parameters. *Journal of Biomechanics*, 29(9):1223–1230.

Fournier, A. (1980). *Génération de mouvements en robotique ; application des inverses généralisées et des pseudo-inverses*. Ph. D. thesis, Montpellier (France).

Hiley M. J. and Yeadon M.R. (2003). Optimum technique for generating angular momentum in accelerated backward giant circles prior to a dismount. *Journal of Applied Biomechanics*, 19:119-130.

Van Soest, A., Gfohler, M. et Casius, L. (2005). Consequences of ankle joint fixation on FES cycling power output : A simulation study. *Medicine and Science in Sports and Exercise*, 37(5):797-806.

Wieber, P.-B., Billet, F., Boissieux, L. et Pissard-Gibollet, R. (2006). The HuMAnS toolbox, a homogeneous framework for motion capture, analysis and simulation. In *Ninth International Symposium on the 3D analysis of human movement*.

Yeadon, M.R., Hiley, M.J. (2000). The mechanics of the backward giant circle on the high bar. *Human Movement Science*, 19 (2), pp. 153-173.

Yeadon, M. R. et Brewin, M. A. (2003). Optimised performance of the backward longswing on rings. *Journal of Biomechanics*, 36(4):545-552.